

Experimental Evaluation of Failure Zone in Sand Beneath the Ring Footing and Cutting Edge of Open Caisson using Image Analysis

Jitesh T. Chavda¹[0000-0003-0396-5759] and G. R. Dodagoudar²

¹Applied Mechanics Department, SVNIT Surat, Surat 395007, India

²Department of Civil Engineering, IIT Madras, Chennai 600036, India
jiteshchavda03@yahoo.in, goudar@iitm.ac.in

Abstract. The analytical evaluation of the bearing capacity of the ring footing and cutting edge of the open caisson requires a definition of the size of failure zone in the soil. Whereas the failure zone in soil depends on the type of soil and the configuration of the ring footing and cutting edge of the open caisson. In the study, the 1g model tests are carried out to evaluate the failure zone in the sand beneath the ring footing and cutting edge of the circular open caisson. The radii ratio of the ring footing and cutting edge of the open caisson models are varied as $r_i/r_o = 0.615, 0.737$ and 0.783 and the tapered angle of cutting edge models are varied as $S = 30^\circ$ and 45° . The radius ratio is the ratio of internal radius to the external radius of the ring footing and cutting edge of the open caisson. The ring footing and caisson models are fabricated using Teflon tubes and Indian standard sand is used as soil medium. The image-based deformation measurement technique is used to evaluate the failure zone in sand. The image analysis results are validated from the rigid displacement test.

Keywords: Ring footing, Open caisson, 1g model test, Cutting edge, Image analysis, Failure zone

1 Introduction

Open caissons are provided with a cutting edge at the bottom to allow the failure of the soil within the caisson and subsequent sinking. The cutting edge has a sloping angle with respect to the vertical face of the cutting edge. This sloping angle is called as tapered angle (S). The tapered angle of the cutting edge can varies from $S = 30$ to 90° . It is noted that the cutting edge with flat base (i.e., $S = 90^\circ$) represents the ring footing. Ring footings are used as foundations to support the structures with symmetrical geometries such as silos, storage tanks, chimneys, cooling towers, bridge piers, etc. The use of ring footing decreases the amount of material usage; hence they are economical apart from providing a beneficial effect of arching.

The bearing capacity of the cutting edge of open caisson and ring footing depends on the size of the failure zone i.e., influence zone. Whereas the size of influence zone depends on the type of soil, configuration of the cutting edge, width and radii ratio of

the ring footing and caisson. The bearing capacity factors of the cutting edge of the open caisson for a predefined influence zone are evaluated by limit equilibrium method (Berezantsev, 1952; Solov'ev, 2008; Yan *et al.*, 2011). However, the different configuration of the cutting edge i.e., variation in the tapered angles of the cutting edge is not explicitly accounted in their study. It is noted that only one study reports the experimental evaluation of the influence zone in sand for varying tapered angles of the cutting edge considering plane strain idealization (Royston *et al.*, 2016). The bearing capacity of ring footing is evaluated by experimental investigations (Saha, 1978; Clark, 1998; Ohri *et al.*, 1997; Saran *et al.*, 2003; Boushehrian and Hataf, 2003; Hataf and Razavi, 2003), the limit equilibrium method, the upper and lower bound plastic limit analyses (Kumar and Chakraborty, 2015), the method of characteristics (Kumar and Ghosh, 2005; Gholami and Hosseininia, 2017), the finite difference method (Zhao and Wang, 2008; Benmebarek *et al.*, 2012; Remadna *et al.*, 2016; Hosseininia, 2016; Benmebarek *et al.*, 2017) and the finite element method (Choobbasti *et al.*, 2010; Lee *et al.*, 2016a; Lee *et al.*, 2016b; Chavda and Dodagoudar, 2019; Tang and Phoon, 2018). In the above mentioned studies, the bearing capacity of the footing depends on the size of failure zone used in the study. However, the literature on the experimental evaluation of the influence zone in soil beneath the cutting edge and ring footing is limited.

In many projects, the large diameter caissons ($D_o > 10$ m) are used (e.g., Nonveiller, 1987; Allenby *et al.*, 2009; Yao *et al.*, 2014; Royston *et al.*, 2016; Sheil *et al.*, 2018). In such projects, the sequential excavation is adopted for the uniform and control sinking of the caisson. A rough estimation of the extent of the influence zone in the soil based on the configuration of the cutting edge and the soil type helps in proper planning of sequential excavation strategies (Nonveiller, 1987). In the present study, the formation of soil displacements field (i.e., influence zone) is evaluated when the caisson ($\alpha = 30$ and 45°) and ring footing ($\alpha = 90^\circ$) models are penetrated in the sand. The image-based deformation measurement technique is used in the study. The experimentally evaluated influence zone in sand beneath the cutting edge and ring footing are normalized by dividing the radial extent of the influence zone with the width of the cutting edge and ring footing. These normalized influence zones can be used in the analytical evaluation of the bearing capacity of the cutting edge and ring footing.

2 Experimental Program

2.1 Apparatus

In order to fully assess the soil displacement field i.e., influence zone, the progressive monitoring of the soil movement is of crucial importance until the required depth of penetration of the caisson and ring footing models is achieved. In order to assess the zone of influence, the image-based deformation measurement technique is used to track the particle movement around the half-cut caisson models. The images are captured through a viewing window of the tank. The caisson model is fixed such that

its cut planar face is parallel and in contact with the viewing window of the tank. This particular arrangement of the test is shown in Fig. 1. The cutting edge of the caissons is embedded in the sand to represent the field conditions. The relative displacement between the camera and the tank is fully arrested during the test, i.e., the tank and the camera are moving upward with the same strain rate whereas the half-open caisson model is stationary. Indirectly the captured photographs show the penetration of the half-open caisson in the sand medium.

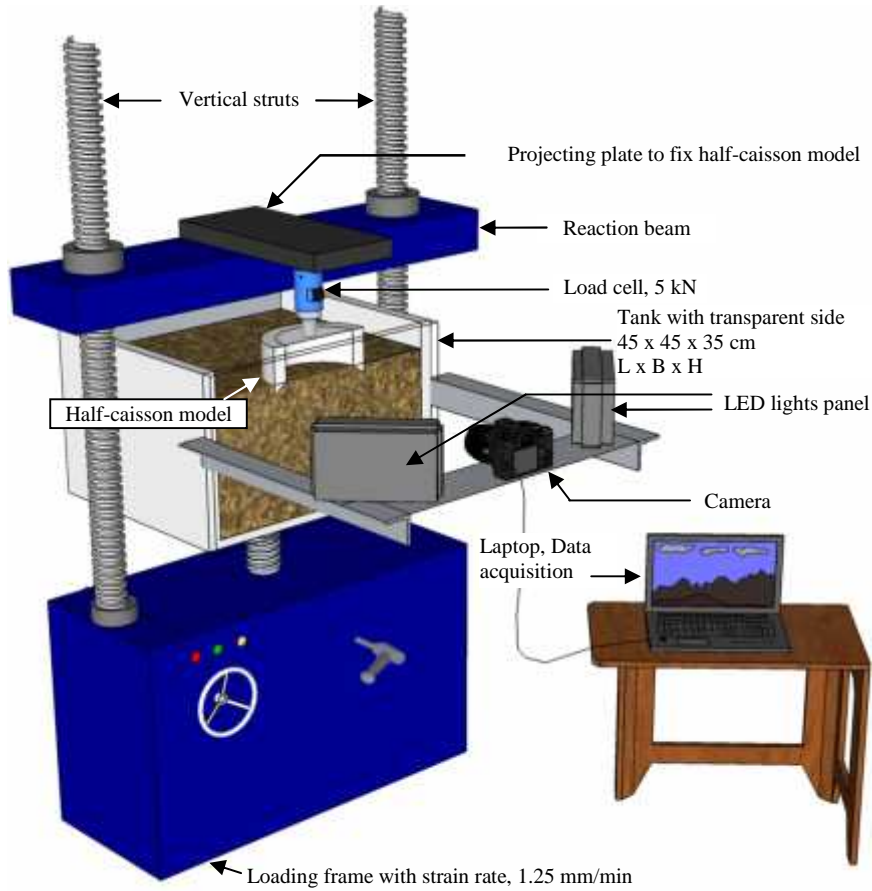


Fig. 1. Experimental setup of caisson model test (Chavda *et al.*, 2019)

2.2 Sand Sample, Caisson and Ring Footing Models

Grade II, Indian standard (IS) sand has been used for all the model tests (IS: 650, 1991). The properties of the sand are given in Table 1. During the entire experimental investigations, the relative density of the sand is maintained as $D_r = 50\%$ in order to limit the scope of the study to one density. For the image-based deformation measurement analysis, the sand texture has been optimized to maximize the precision in the measurement of the soil displacements (White *et al.*, 2003; Take, 2003; White

and Take, 2005; Stanier and White, 2013). The procedure reported in Chavda *et al.* (2019) is used for the preparation of the dyed sand and the methodology to achieve the optimum texture. The texture is generated by mixing the IS sand with 65% of dyed sand by weight. The sand used in all the experiments comprises of 35% of the IS sand and 65% of the dyed sand. The dyed sand is prepared by mixing the black color ink with IS sand such that the geotechnical properties of the dyed sand are not altered.

For the image analysis, the caisson models are half-cut to represent an axisymmetric problem. The transparent side of the tank is made of Perspex acrylic sheet. For maximum repetitive use of the transparent acrylic sheet, the caisson and ring footing models are fabricated with Teflon tubes for the investigation of the soil displacement field. The models has unit weight = 11 kN/m³, Young's modulus = 500 MPa and Poisson's ratio = 0.46. The Young's modulus of the caisson models is almost 80 times higher than the sand ($E = 5.768$ MPa) and hence the models are relatively rigid and hence they experience negligible deformations.

Table 1. Index properties of Indian standard sand, Grade II

Parameter	Unit	Value
Specific gravity	-	2.64
Max. unit weight	kN/m ³	16.81
Min. unit weight	kN/m ³	14.50
Relative density	%	50
Unit weight of sand	kN/m ³	15.57
Unified soil classification	-	SP ^a

^aSP - Poorly graded sand

2.3 Data Processing

The soil displacement field around the cutting edge of the open caisson and ring footing is examined by performing the image-based deformation measurement analysis using the open source MATLAB program, GeoPIV-RG (White *et al.*, 2003; Stanier and White, 2013; Stanier *et al.*, 2016). The GeoPIV-RG follows the principle of particle image velocimetry (PIV), originally developed in the field of experimental fluid mechanics (Adrian, 1991). Certain modifications to the PIV technique have been proposed by White *et al.* (2003) and Stanier *et al.* (2016) to enhance its applicability in geotechnical engineering. The images obtained from the tests consist of series of images from the initial to the final penetration depth i.e., up to the penetration depth same as the half-width of the cutting edge and ring footing. The resistance load of the caisson is reached to the ultimate value (i.e., the failure load) corresponding to the penetration depth lesser than half-width of the cutting edge having $\delta = 30$ to 90° (Chavda *et al.*, 2019). In the study, the influence zone in the soil is obtained corresponding to the penetration depth of half-width of the cutting edge and ring footing.

2.4 Test Procedure

In the present study, a Nikon D5300 digital single-lens reflex camera is used for image analysis. An external lighting is provided by the two 16W LED light panels as shown in Fig. 1. The test is performed by moving the tank in the upward direction with a constant strain rate of 1.25 mm/min and the photographs are captured at an interval of 3 seconds (0.33 Hz). This frequency of image acquisition is decided based on the strain rate and displacement of the soil medium between the two successive images. The tests are stopped when the penetration of the models reach the penetration same as the half-width of the cutting edge and the ring footing.

The test results are validated by performing rigid displacement test. In the test, the tank is moved in the upward direction at the same strain rate of 1.25 mm/min and the rigid displacement of the tank is measured from the dial gauge positioned over the pedestal. At the same time, the displacement of the tank is also captured by the camera. The vertical displacement is calculated from the GeoPIV-RG program and the same is also noted from the dial gauge. From this test, it is found that the displacements obtained from the GeoPIV-RG program are predicted within the error range of $\pm 3\%$ of the dial gauge readings.

2.5 Evaluation of Size of Failure Zone

The vectorial displacement plots and horizontal displacement plots corresponding to the penetration depth of $0.5B$ is obtained from GeoPIV_RG. In the horizontal displacement plot, only the radial inward horizontal displacement vectors are plotted in order to get the clear picture of the failure zone. The typical plot of the vectorial displacement, horizontal displacement contours, and the radial inwards displacement contours are shown in Fig. 2 corresponding to the cutting edge having radius ratio of 0.783 and the tapered angle of 60° . The failure zone is evaluated from these three plots corresponding to the penetration results of cutting edge and ring footing. The influence zone are normalised by diving the radial and vertical extent of the failure zone by the width of the cutting edge and ring footing. Thus the failure zone obtained is called normalised influence zone.

3 Results and Discussion

In the study, the shear strain (\dagger) of 10% and 20% is also evaluated. The region of soil between the shear strain value of $\dagger = 10\%$ and 20% represents the soil whose shear strain is mobilized up to 20%. In the present study, the normalized failure zone and the shear strain = 20% is presented for varying radii ratio ($r_i/r_o = 0.615, 0.737,$ and 0.783) and different tapered angles ($S = 30, 45$ and 90°) of the cutting edge. The tapered angle $S = 90^\circ$ represents the ring footing.

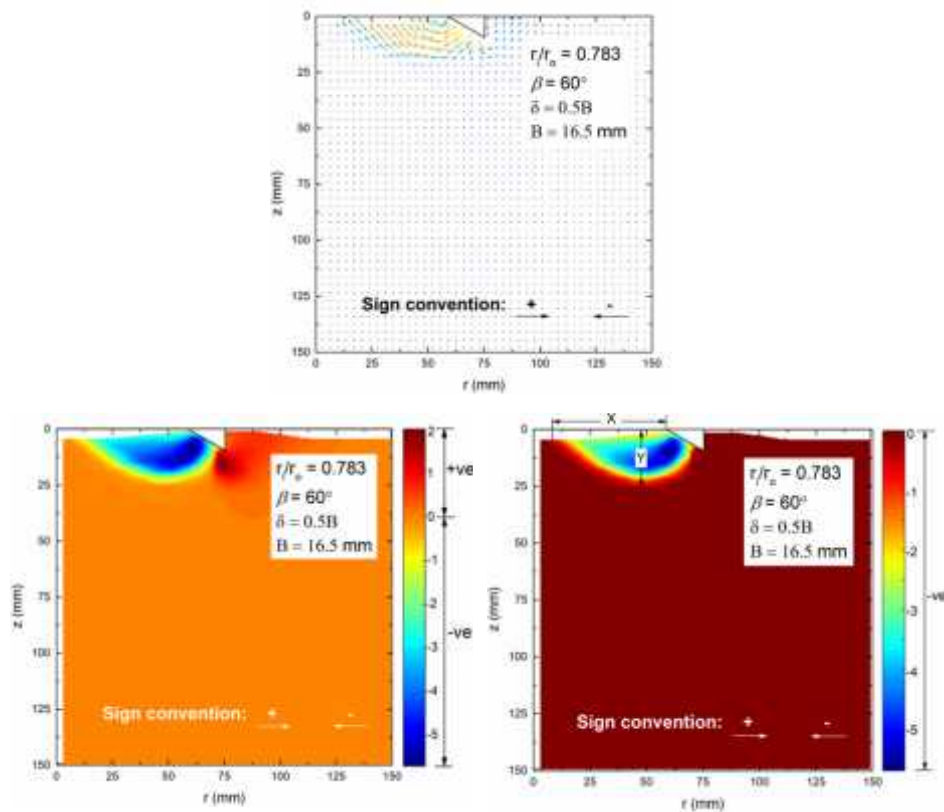


Fig. 2. Typical vectorial displacement, horizontal displacement contour, and the radial inward displacement contour plots

3.1 Failure Zone: Ring Footings

The failure zones in the sand beneath the ring footings obtained from the image analysis for varying radii ratio are shown in Fig. 3. It is seen from the figure that with increase in the radii ratio, the failure zone tends to move away from the centroidal axis of the ring footing. It is also noted that the failure zone tends to move asymmetric failure zone to symmetric failure zone with increase in the radii ratio of the ring footing. Hence, it is opined that with increase in the radii ratio of ring footing nearly to 1, the failure zone will be similar to the strip footing having width same as the width of the ring footing. The size of failure zone is less within the ring footing and it increases with increase in the radii ratio. Whereas, the size of failure zone outside the ring footing increases with increase in the radii ratio. At lower value of radius ratio ($r_i/r_o = 0.615$), the size of failure zone within footing is lesser than the size of failure zone outside the footing. This is possibly due to the arching action i.e., more volume of soil, present outside the footing, contributes the capacity of the footing.

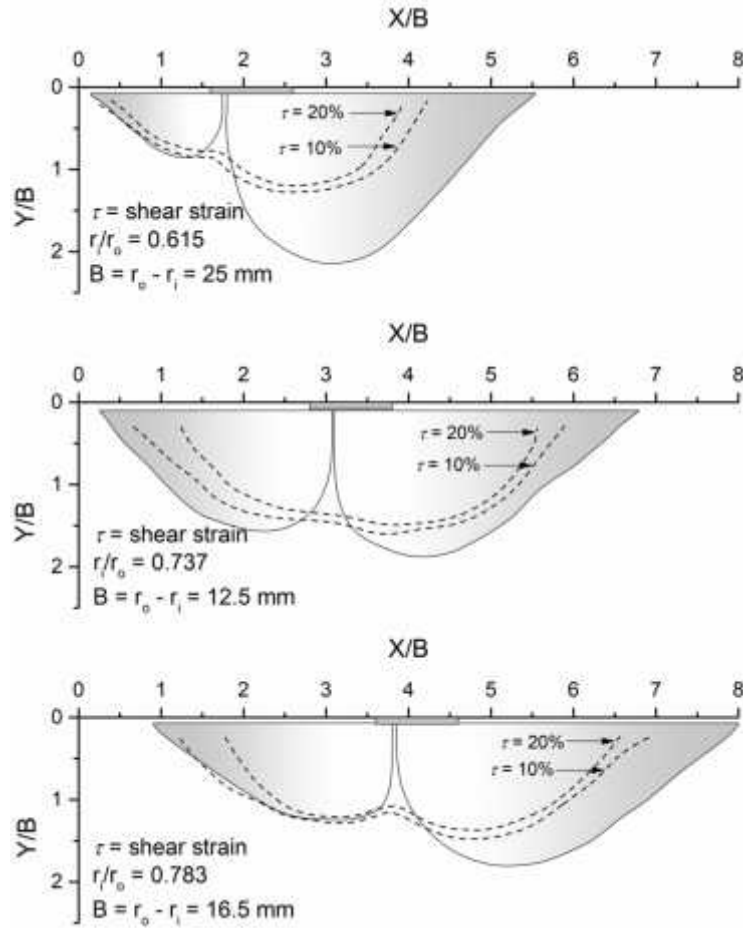


Fig. 3. Failure zone in sand beneath ring footing

3.2 Failure Zone: Cutting edge of Open Caisson

The failure zones in the sand beneath the cutting edge of circular open caisson obtained from the image analysis for varying radii ratio and different tapered angles are shown in Fig. 4. It is seen from the figure that with increase in the radii ratio, the size of the failure zone increases for both the tapered angles of cutting edge. However, the size of failure zone is higher for $S = 30^\circ$ compared to the cutting edge with $S = 45^\circ$. The region of soil whose shear strain is mobilized up to 20% tends to move outside the cutting edge for $S = 45^\circ$ compared to the cutting edge with $S = 30^\circ$. The failure zone is attributed within the caisson only when steeper cutting edges are used (i.e., $S = 30^\circ$).

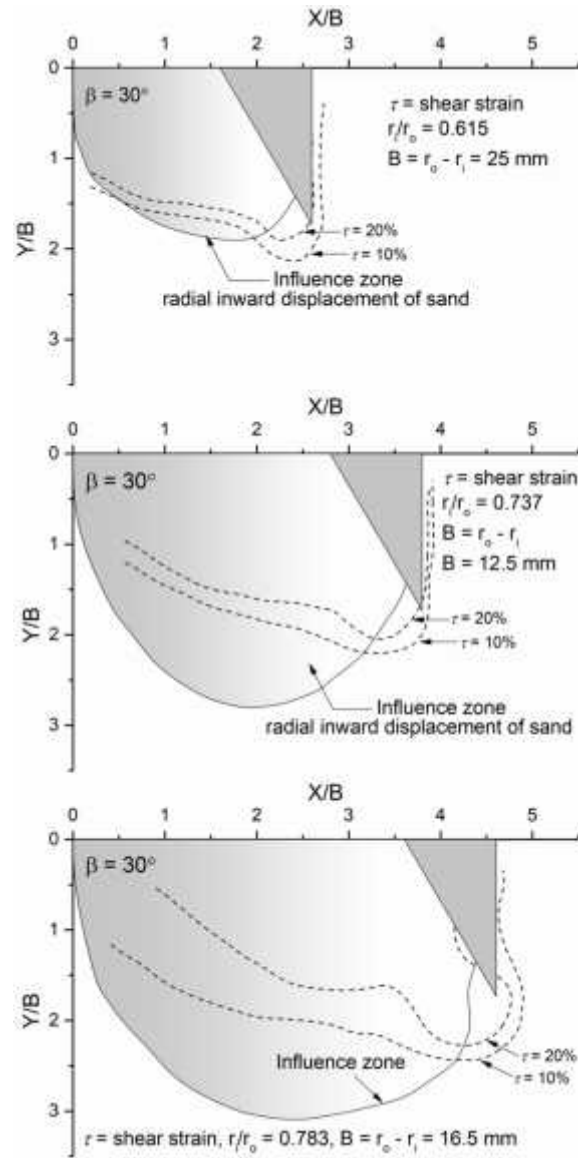


Fig. 4. (continued on next page)

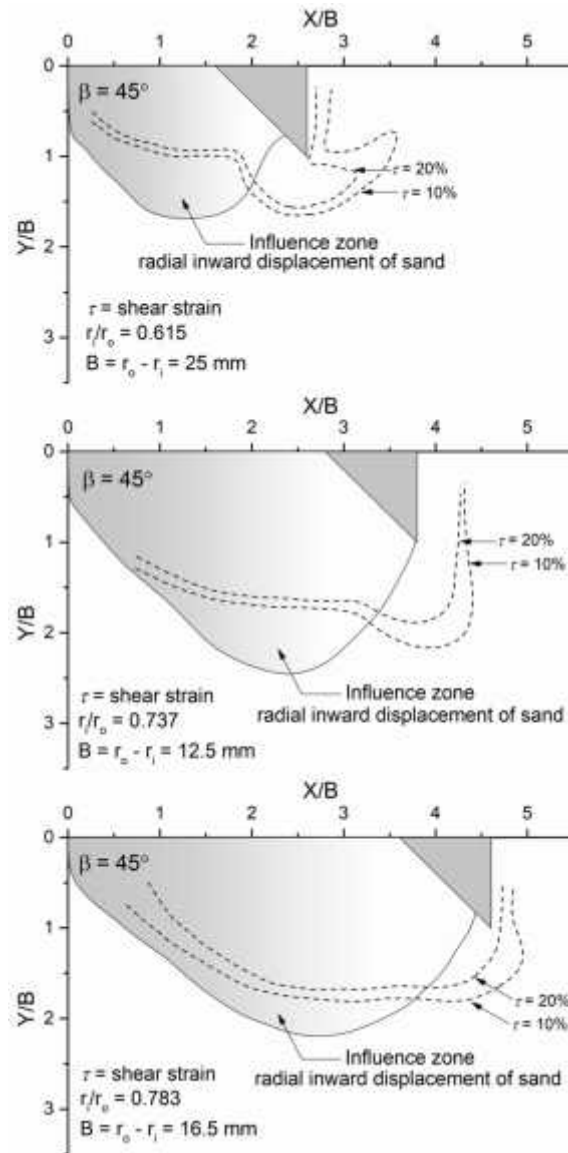


Fig. 4. Failure zone in sand beneath cutting edge of open caisson

4 Conclusions

In the study, the $1g$ model tests are carried out and the failure zone in the sand beneath the ring footing and cutting edge of circular open caisson is evaluated. The caisson and ring footing models are fabricated with varying radii ratio ($r_i/r_o = 0.615$, 0.737 , and 0.783) and caisson has cutting edge with two different tapered angles ($S =$

30 and 45°). The present study results can be used in the analytical studies in determination of the bearing capacity of the cutting edge and ring footing. The following conclusions are drawn from the experimental investigations.

- The failure zones in sand beneath the ring footing and cutting edge of circular open caisson are evaluated using image processing technique.
- At lower value of radius ratio = 0.615, the size of failure zone in sand is less within the ring footing compared to the size of failure zone in sand outside the ring footing. The size of failure zone in sand within ring footing increases with increase in the radii ratio of the footing. The failure zone tends to move asymmetric failure zone to symmetric failure zone with increase in the radii ratio of the ring footing.
- The size of the failure zone in the sand beneath the cutting edge of caisson increases with increase in the radii ratio for both the tapered angles of the cutting edge. The size of the failure zone decreases with increase in the tapered angles of the cutting edge. The steeper cutting edge has higher capacity than the flatter cutting edge. The steeper cutting edges restrict the failure of soil within the caisson only.

The mean stress level can influence the failure process of the granular material. For the usage of results in practice, the failure zone obtained in the study are normalised by the width of the cutting edge. However, it is opined that the further consideration of scaling effects can be made by a comprehensive numerical approach to calibrate the model with the experimental results and extrapolated later to the real-field situations.

References

1. Adrian RJ (1991) Particle imaging techniques for experimental fluid mechanics. *Annual Review of Fluid Mechanics*, 23:261–304.
2. Allenby D, Waley G, Kilburn D (2009) Examples of open caisson sinking in Scotland. *Proceedings of the ICE - Geotechnical Engineering*, 162(1):59-70.
3. Benmebarek S, Saifi I, Benmebarek N (2017) Undrained vertical bearing capacity factors for ring shallow footings. *Geotechnical and Geological Engineering*, 35(1):355-364.
4. Berezantsev (1952) Axisymmetric problem of the theory of limiting equilibrium of granular media. Gosstroizdat, Moscow [in Russian].
5. Boushehrian JH, Hataf N (2003) Experimental and numerical investigation of the bearing capacity of model circular and ring footings on reinforced sand. *Geotextiles and Geomembranes*, 21(4):241–256.
6. Chavda JT, Dodagoudar GR (2019). Finite element evaluation of vertical bearing capacity factors N'_c , N'_q and N'_x for ring footings, *Geotechnical and Geological Engineering*, 37(2):741-754.
7. Chavda JT, Mishra SR, Dodagoudar GR (2019) Experimental evaluation of ultimate bearing capacity of the cutting edge of open caisson, *International Journal of Physical Modelling in Geotechnics*, doi: 10.1680/jphmg.18.00052.

8. Choobbasti AJ, Hesami S, Najafi A, Pirzadeh S, Farrokhzad F, Zahmatkesh A (2010) Numerical evaluation of bearing capacity and settlement of ring footing; case study of Kazeroon cooling towers. *International Journal of Research and Reviews in Applied Sciences*, 4(3):263–271.
9. Clark JI (1998) The settlement and bearing capacity of very large foundations on strong soils: 1996 RM Hardy keynote address. *Canadian Geotechnical Journal*, 35(1):131–145.
10. Gholami H, Seyedi Hosseininia E (2017) Bearing capacity factors of ring footings by using the method of characteristics, *Geotechnical and Geological Engineering*, 35(5):2137-2146.
11. Hataf N, Razavi MR (2003) Behavior of ring footing on sand. *Iranian Journal of Science and Technology Transactions B: Engineering*, 27:47–56.
12. IS: 650 (1991) Standard sand for testing cement - Specification. Bureau of Indian Standards, New Delhi.
13. Kumar J, Chakraborty M (2015) Bearing capacity factors for ring foundations. *Journal of Geotechnical and Geoenvironmental Engineering*, 141(10):06015007-1-7.
14. Kumar J, Ghosh P (2005) Bearing capacity factor N_γ for ring footings using the method of characteristics. *Canadian Geotechnical Journal*, 40(3):1474–1484.
15. Lee JK, Jeong S, Lee S (2016a) Undrained bearing capacity factors for ring footings in heterogeneous soil. *Computers and Geotechnics*, 75:103–111.
16. Lee JK, Jeong S, Shang JQ (2016b) Undrained bearing capacity of ring foundations on two-layered clays. *Ocean Engineering*, 119:47–57.
17. Nonveiller E (1987) Open caissons for deep foundations. *Journal of Geotechnical Engineering*, ASCE, 113(5):424-439.
18. Ohri ML, Purhit DGM, Dubey ML (1997) Behavior of ring footings on dune sand overlaying dense sand. *Proceedings of International Conference of Civil Engineering*, Tehran, Iran, 4-6.
19. Royston R, Phillips BM, Sheil BB, Byrne BW (2016) Bearing capacity beneath tapered edges of open dug caissons in sand. *Proceedings of Civil Engineering Research in Ireland*, Galway, Ireland.
20. Saha MC (1978) Ultimate bearing capacity of ring footings on sand. Masters in Engineering Thesis, University of Roorkee, Roorkee.
21. Saran S, Bhandari NM, Al Smadi MMA (2003) Analysis of eccentrically obliquely loaded ring footings on sand. *Indian Geotechnical Journal*, 33(4):422–446.
22. Solov'ev NB (2008) Use of limiting-equilibrium theory to determine the bearing capacity of soil beneath the edges of caissons. *Soil Mechanics and Foundation Engineering*, 45(2):39-45.
23. Stanier SA, Blaber J, Take WA, White DJ (2016) Improved image-based deformation measurement for geotechnical applications. *Canadian Geotechnical Journal*, 53(5):727–739.
24. Stanier, S. A, White D. J. (2013) Improved image-based deformation measurement for the centrifuge environment. *Geotechnical Testing Journal*, 36(6):915-927.
25. Sheil B, Royston R, Byrne B (2018) Real-time monitoring of large-diameter caissons. *Proceedings of China-Europe Conference on Geotechnical Engineering*, 725-729, https://doi.org/10.1007/978-3-319-97112-4_162.
26. Take W (2003) The influence of seasonal moisture cycles on clay slopes, Ph.D. Thesis, University of Cambridge, Cambridge, U.K.
27. Tang C, Phoon KK (2018) Prediction of bearing capacity of ring foundation on dense sand with regard to stress level effect. *International Journal of Geomechanics*, ASCE, 18(11):04018154.

28. White DJ, Take WA, Bolton MD (2003) Soil deformation measurement using particle image velocimetry (PIV) and photogrammetry. *Géotechnique*, 53(7):619-631.
29. White DJ, Take WA (2005) Discussion on: Application of particle image velocimetry (PIV) in centrifuge testing of uniform clay by Zhang Y. D., Tan T. S. and Leung C. F. *International Journal of Physical Modelling in Geotechnics*, 5(4):27-31.
30. Yan FY, Guo YC, Liu SQ (2011) The bearing capacity analyses of soil beneath the edge of circular caisson. *Advanced Materials Research*, 250:1794-1797.
31. Yao Q, Yang X, Li H (2014) Construction technology of open caisson for oversize surge shaft in drift gravel stratum, *Electronic Journal of Geotechnical Engineering*, 19:5725-5738.
32. Zhao L, Wang JH (2008) Vertical bearing capacity for ring footings. *Computers and Geotechnics*, 35(2):292-304.